Comparative Oxidation Studies of Methionine Residues Reflect a Structural Effect on Chemical Kinetics in rhG-CSF†

Bin Pan,‡ Jeff Abel,§ Margaret S. Ricci,§ David N. Brems,§ Daniel I. C. Wang,‡ and Bernhardt L. Trout*,‡

Department of Chemical Engineering, Massachusetts Institute of Technology, 77 Massachusetts Avenue, Room E19-502B, Cambridge, Massachusetts 02139, and Pharmaceutics Department, Amgen Inc., Thousand Oaks, California 91320

Received September 5, 2006; Revised Manuscript Received October 23, 2006

ABSTRACT: The effect of protein conformation on the rate of chemical degradation is poorly understood. To address the role of structure on chemical degradation kinetics, comparative oxidation studies of methionine residues in recombinant human granulocyte colony-stimulating factor (rhG-CSF) were performed. The kinetics of oxidation of methionine residues by hydrogen peroxide (H_2O_2) in rhG-CSF and corresponding chemically synthesized peptides thereof was measured at different temperatures. To assess structural effects, equilibrium denaturation experiments also were conducted on rhG-CSF, yielding the free energy of unfolding as a function of temperature. A comparison of the relative rates of oxidation of methionine residues in short peptides with those of corresponding methionine residues in rhG-CSF yields an understanding of how protein tertiary structure affects oxidation reactions. For the temperature range that was studied, 4−45 °C, the oxidation rate constants followed an Arrhenius equation quite well, suggesting the lack of temperature-induced local structural perturbations that affect chemical degradation rates. One of the four methionine residues, Met 122, exhibited an activation energy significantly different from that of the corresponding peptide. Extrapolation of kinetic data predicts non-Arrhenius behavior around the melting temperature. Three phenomenological models based on different mechanisms are discussed, and an application to shelf life prediction of pharmaceuticals is presented.

The oxidation of methionine amino acids is an important reaction for proteins both in vivo and in vitro. In vivo, a number of processes of biological interest involve methionine oxidation, such as aging (*1*−*3*), Parkinson's disease (*4*), and Alzheimer's disease (*5*, *6*). In addition, the oxidation of a methionine residue and its reduction by methionine sulfoxide reductase are thought to be a regulatory mechanism for enzyme bioactivity (*7*, *8*). In vitro, oxidation is important in the production of protein pharmaceuticals. An inevitable problem for these protein molecules in aqueous solution is the various physical and/or chemical degradation reactions that occur during the shelf life of the product (*9*). Oxidation is one of the common chemical degradation pathways, often resulting in structural changes (*10*) and bioactivity losses (*11*). Minimizing oxidation as well as other forms of degradation is essential in formulating pharmaceutical proteins (*12*).

At ambient temperature and at physiological temperature, the oxidation rate constants of different methionine residues in a given protein, such as G-CSF[1] (*13*) and human α1-antitrypsin (*14*), can differ by an order(s) of magnitude. Chu et al. (*13*, *15*−*17*) explained this observation with the introduction of a new mechanism for methionine oxidation in proteins by hydrogen peroxide. In this mechanism, water molecules play an important role in stabilizing the transition state. They also found that (*13*, *15*−*17*) solvent accessible area is not sufficient to distinguish the disparate oxidation rate constants among methionine residues, as previously thought. Instead, they proposed a new structural quantity, ensemble-averaged two-shell water coordination number, derived from molecular dynamics simulations, which was found to correlate well with oxidation rate constants. An obvious next question then is how local variations in amino acids near a given methionine site affect oxidation in the absence of structural effects. There are two ways of addressing this question: through equilibrium denaturation experiments and by studying peptides that have the same sequence in the local region around each methionine residue of interest. In this paper, we report the results of both kinds of studies, performed on the very important therapeutic protein G-CSF. Comparative kinetics studies were conducted using rhG-CSF and synthetic peptides, which were synthesized to mimic the local sequence around methionine residues in rhG-CSF. The differences in methionine oxidation rate constants as a function of temperature were obtained from experimental measurements, and a correlation with free energies of equilibrium denaturation of rhG-CSF at different temperatures was made.

rhG-CSF is a four-helix bundle protein with 175 amino acid residues (*18*), containing four methionine residues. The crystal structure (*19*, *20*) is shown in Figure 1, and all four methionine residues are highlighted in a ball-stick represen-

† We gratefully thank Amgen Inc. for funding this project.

* To whom correspondence should be addressed. Phone: (617) 258-5021. Fax: (617) 253-2272. E-mail: trout@mit.edu.

‡ Massachusetts Institute of Technology.

§ Amgen Inc.

[1] Abbreviations: CD, circular dichroism; DTT, dithiothreitol; G-CSF, granulocyte colony-stimulating factor; LC, liquid chromatography; MS, mass spectrometry; rhG-CSF, recombinant human granulocyte colony-stimulating factor; TFA, trifluoroacetic acid.

10.1021/bi061855c CCC: $33.50
Published on Web 12/07/2006

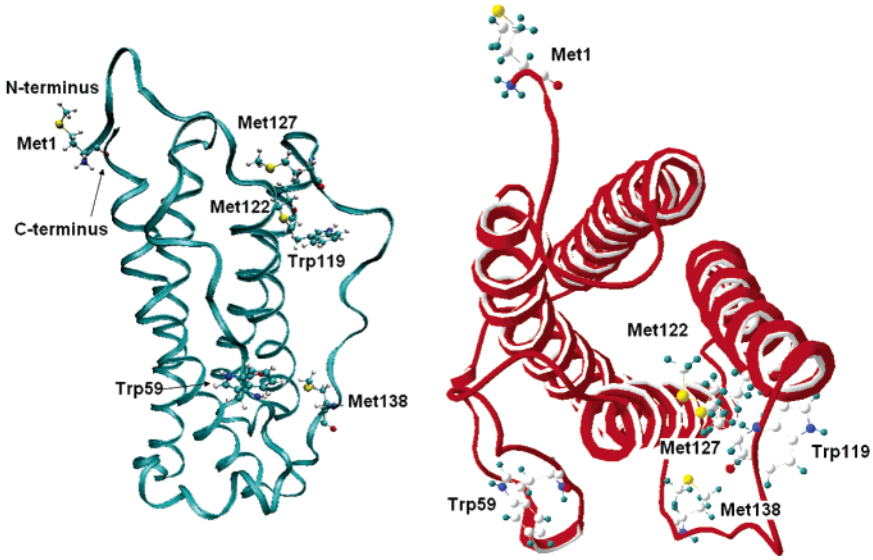

FIGURE 1: Crystal structure of rhG-CSF from refs *19* and *20*. Four N-terminal residues missing in the X-ray structure (PDB entry 1cd9), MTPL, were added. Their atomic position in space was determined by minimizing the potential energy in vacuum using the CHARMM force field, with the constraints being that all known atomic positions from the X-ray structure were fixed.

tation; its main chain backbone is shown in a ribbon representation. Met 1 is at the N-terminus, encoded by the initiation codon in protein synthesis, and is therefore very flexible. Met 122 is within helix C, facing the interior and buried to a great extent. Met 127 and Met 138 both face the protein interior and are located in the B−C loop, which is more flexible than the helix that contains Met 122. Also shown in Figure 1 is the location of the two tryptophan residues, Trp 59 and Trp 119, which serve as fluorescence spectral probes of the local environment. Trp 59 resides in the long A−B loop between helices A and B with its side chain pointing out toward solvent, whereas Trp 119 resides within helix C with its side chain between the interface of helix C and the C−D loop. Trp 59 is far from all of the methionine residues and is much exposed despite its hydrophobic nature, while Trp 119 is close to Met 122 and is significantly buried. However, neither of the two tryptophan residues has a similar microenvironment like any of the methionine residues.

MATERIALS AND METHODS

Materials. rhG-CSF expressed and produced in *Escherichia coli* was provided by Amgen Inc. Three short peptides with sequences which mimic the corresponding sequences in rhG-CSF around Met 122, Met 127, and Met 138 were synthesized by SynPep Co. The peptide sequences are acetyl-QQMEEY-$CONH_2$ (denoted pep1 and corresponding to Met 122), acetyl-LGMAPY-$CONH_2$ (denoted pep2 and corresponding to Met 127), and acetyl-GAMPAY-$CONH_2$ (denoted pep3 and corresponding to Met 138), all of which were acetylated at the C-terminus and tagged with a tyrosine residue at the N-terminus. Ultrapure guanidinium hydrochloride was purchased from MP Biomedicals (catalog no. 105696). All other chemicals were purchased from Sigma Aldrich.

Oxidation Kinetics Measurement for Peptides. A mixture of 0.5 mg/mL rhG-CSF with equimolar concentrations of the three short peptides was prepared in 10 mM acetate buffer at pH 4.0. Ionic strength was adjusted to 100 mM by adding NaCl. Concentrated hydrogen peroxide [30% (w/w) H_2O_2] was added to the mixture solution at different concentrations at different temperatures. The actual concentration of the stock solution of H_2O_2 [labeled 30% (w/w)] purchased from Sigma-Aldrich was determined by following the UV−vis absorbance at 240 nm using an extinction coefficient of 43.6 (the detailed procedure is contained in the Production Information Sheet). In all cases, hydrogen peroxide is in large excess, with H_2O_2:rhG-CSF molar ratios ranging from 1:500 to 1:3000. Reaction mixtures were incubated at a range of temperatures, from 4 to 50 °C in a water bath. After addition of hydrogen peroxide and incubation at a specified temperature, aliquots of the reaction mixture were removed at different time points and the remaining hydrogen peroxide was quenched with catalase (Sigma catalog no. c9284). Samples were then centrifuged, and there were no considerable soluble aggregates in these samples up to the end of oxidation as verified by size exclusion chromatography. In addition, there was full recovery with respect to total peak area, suggesting no loss due to insoluble materials. The supernatant was divided into two halves, one for the quantification of the oxidation kinetics of the short peptides and the other for the Glu-C peptide map of rhG-CSF.

The sample for the quantification of the oxidation kinetics of the short peptides was analyzed by RP-HPLC using an Agilent 1100 series instrument or Beckman Coulter Gold with a C_4 column (Phenomenex, Jupiter 5 μm C_4, 300 Å, 150 mm × 4.6 mm). The mobile phases were 0.1% TFA in water (A) and 90% acetonitrile with 0.1% TFA in water (B). The column was equilibrated with 10% B initially. After the sample was injected, the separation was achieved by a linear gradient from 10 to 40% B for 20 min, a gradient from 40 to 80% B for 30 min, a constant concentration of B of 80% for 5 min, and back to 10% for an additional 10 min. The column temperature was controlled at 60 °C, and the flow rate was 0.8 mL/min. The absorbance signal was monitored by a visible−ultraviolet diode array detector at a wavelength of 214 nm.

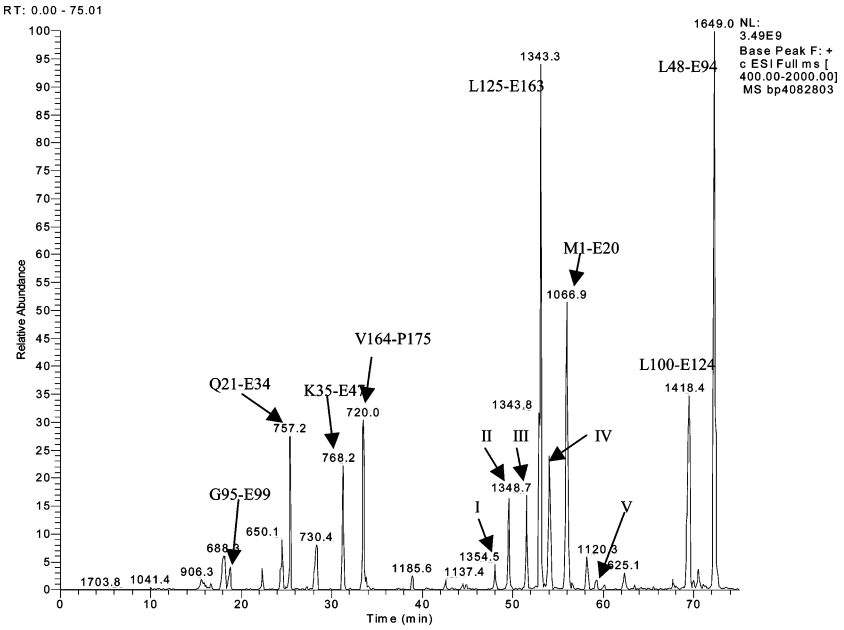

FIGURE 2: Mass spectrum of Glu-C-digested peptide fragments. The number over each peak refers to the molecular weight of the fragment, with the fragment identification in rhG-CSF indicated by an arrow: (I) L125−E163 with M138(O) and M127(O), (II) L125−E163 with M127(O), (III) L125−E163 with M138(O), (IV) M1−E20 with M1(O), and (V) L100−E124 with M122(O).

Peptide Mapping and Oxidation Kinetics Measurement for rhG-CSF. The sample used for rhG-CSF quantification was first digested with Glu-C endoproteinase. Glu-C endoproteinase selectively cleaves at the C-terminal side of glutamate sites in protein molecules under reducing buffer conditions. The digestion buffer was comprised of 0.5 M Tris, 0.5 M Tris-HCl, 0.4 M methylamine hydrochloride (CH_3NH_2·HCl), 0.2 M DTT, and 6 M urea. For a typical aliquot of the sample with a volume of 100 μL, 200 μL of digestion buffer and 10 μL of 0.2 μg/μl Glu-C endoproteinase were added, and the whole mixture was incubated at room temperature for 18 ± 1 h. The digested sample was then analyzed by RP-HPLC with a C_4 column (Phenomenex, Jupiter 5 μm, 300 Å, 250 mm × 2.0 mm). The mobile phases were 0.085% TFA in water (A) and 90% acetonitrile with 0.085% TFA in water (B). The column was equilibrated with 2% B initially. After the sample was injected, the separation was achieved with a linear gradient from 2 to 30% B for 30 min, a gradient from 30 to 60% B for 45 min, a gradient from 60 to 98% B for 15 min, a constant concentration of B at 98% for 15 min, and back to 2% B for 12 min. The column temperature was controlled at 40 °C with a flow rate of 0.2 mL/min. The absorbance signal was monitored by a visible−ultraviolet diode array at a wavelength of 214 nm. Most of the oxidation kinetics measurements were performed in duplicate, and it was found that the deviations from fitting to the pseudo-first-order reaction kinetcs were greater than the variations between two different sets of time points. Therefore, the error bars in the reported oxidation rate constants were from the variations in the linear fit to pseudo-first-order reaction kinetics.

LC−MS/MS data were acquired using a model Finnigan LCQ series mass spectrometer with an electrospray interface and XCaliber software from Thermo Electron Co. The data were used to identify each of the digested fragments and the oxidized methionine-containing fragments. As shown in Figure 2, oxidized and unoxidized forms of these methionine-containing fragments can be separated well by HPLC. Among all the major peaks identified using MS/MS, no other oxidized residues such as Trp or Tyr were found. Oxidized forms I−V and unoxidized forms such as L125−E163, M1−E20, and L100−E124 are indicated. The areas under these peaks were used to calculate the oxidation rate constants.

Equilibrium Denaturation Monitored by Intrinsic Fluorescence. Equilibrium denaturation by GdnHCl was performed on rhG-CSF in 10 mM acetate at pH 4.0 over a range of temperatures. An AVIV model ATF105 fluorometer with an automated titration system was used to generate fluorescence data. Two stock protein solutions with a protein concentration of 0.5 mg/mL were prepared with concentrated GdnHCl (approximately 8 M) and no denaturant. The titration system was comprised of a Hamilton pump, which removed a set volume of denatured protein solution from the cuvette and injected an equivalent volume of protein solution from the syringe, decreasing the concentration of GuHCl by 0.1 M for each spectral measurement. After the dilution of the denaturant, the solution in the cuvette was allowed to mix and equilibrate for 3 min at room temperature. The fluorescence intensity was recorded at an excitation wavelength of 280 nm and an emission wavelength of 340 nm, per previous work (*21*).

Equilibrium Denaturation Monitored by Circular Dichroism (CD). The same buffer condition as in fluorescence equilibrium denaturation was used for CD experiments, except that the rhG-CSF concentration was 0.02 mg/mL. A model J810 CD spectrophotometer from JASCO was used. A similar automated titration system was used to prepare mixtures with different denaturant concentrations. The CD signal at 222 nm was collected by SpectraManager.

Data Analysis of Tryptophan Fluorescence and CD Data. Data from equilibrium denaturation experiments were processed according to a standard method developed by Tanford (*22*). Raw CD and fluorescence data were fit to a two-state model for protein unfolding and folding.

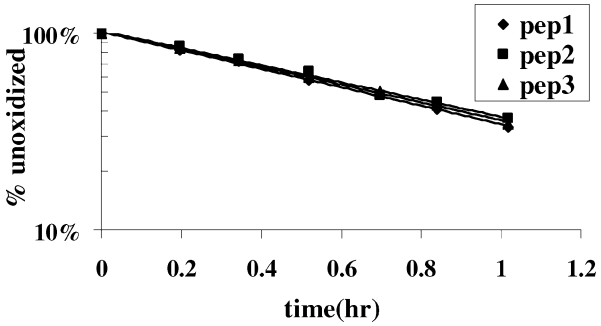

FIGURE 3: Oxidation time-course of short peptides. This graph shows the unoxidized percentage of the three short peptides vs time, under the reaction condition in a pH 4.0, 10 mM sodium acetate buffer at 37 °C. Linear regressions were performed to generate pseudo-first-order rate constants, from which second-order oxidation rate constants were obtained.

RESULTS

Temperature Dependence of Methionine Oxidation Kinetics for Short Peptides. Since a large excess of H_2O_2 was used in the all of the oxidation experiments, its concentration is assumed to be a constant in the calculation of rate constants. As shown in Figure 3, the concentration of unoxidized peptides was normalized to their initial concentrations and plotted on a semilogarithmic scale. Linear fitting (where $R^2 > 0.98$) was performed on this plot to ensure the validity of the assumed pseudo-first-order reaction and to obtain the pseudo-first-order rate constants. The measured rates of methionine oxidation in the short peptides are listed in Table 1. Second-order rate constants were obtained from the division of pseudo-first-order rate constants by the hydrogen peroxide concentration. Figure 4 shows that on the Arrhenius plots, the methionine oxidation rate is nearly independent of sequence in the three peptides. The oxidation rates of methionine residues in these hexapeptides are very close to the oxidation rate of free methionine, suggesting that the primary sequence of these peptides has little effect on their oxidation rate.

Temperature Dependence of the Oxidation Kinetics of Methionine Residues in rhG-CSF. Like the oxidation kinetics analysis for three peptides, the concentration of unoxidized methionine residues was normalized to their initial concentrations and plotted on a semilogarithmic scale, as shown in Figure 5. A procedure similar to that described for the three peptides was carried out to generate the rate constants given in Table 1.

In Table 1, the oxidation rate constants both for the three short peptides and for the four methionine residues in rhG-CSF at different temperatures are listed. The oxidation rate constants vary by more than 2 orders of magnitude among different methionine residues in rhG-CSF. In addition, the oxidation rate constants vary by more than 1 order of magnitude in the temperature range of 4−60 °C for each given methionine residue.

From the data in Table 1, Arrhenius plots were obtained and are shown in Figure 6. Linear regressions were performed according to the Arrhenius equation $k = Ae^{-(\Delta E)/(RT)}$. The values of the Arrhenius parameters, activation energy ΔE and prefactor A, are listed in Table 2. In general, the apparent activation energies and prefactors of three peptides are approximately equal within the experimental errors, while those of methionine resides in rhG-CSF vary significantly. Understanding these differences is essential, as explained later.

Equilibrium Denaturation of rhG-CSF at Different Temperatures. Both fluorescence and CD signals were used to track the structural changes in the equilibrium denaturation and renaturation processes. There are two tryptophan residues in rhG-CSF, Trp 59 and Trp 119 (*23*), that give rise to a fluorescence signal at 340 nm with an excitation wavelength of 280 nm. Figure 7 shows the raw fluorescence data that were converted to fraction of unfolded protein by fitting to a two-state model versus the concentration of GdnHCl for different temperatures. From approximately 2 °C to 10 °C, the denaturation midpoints shifted toward higher GdnHCl concentrations and then backward to lower GdnHCl concentrations at higher temperatures, therefore exhibiting a maximum stability temperature. A quantitative description of the position of each curve can be described by the midpoint denaturant concentration, C_m (*22*), and the m value.

The results from CD and tryptophan fluorescence are listed in Table 3. The definitions of the m value and C_m follow those of Tanford (*22*).

Fit to the Gibbs−Helmholtz Equation. From a well-known thermodynamic relation, one has

$$\left(\frac{\partial \frac{\Delta G}{T}}{\partial \frac{1}{T}}\right)_P = \Delta G - T\left(\frac{\partial \Delta G}{\partial T}\right)_P = \Delta G + T\Delta S = \Delta H \quad (1)$$

While for small molecules, it is quite safe to assume ΔH is constant

$$\left(\frac{\partial \frac{\Delta G}{T}}{\partial \frac{1}{T}}\right)_P = -R\left[\frac{\partial \log(K)}{\partial \frac{1}{T}}\right]_P = \Delta H \quad (2)$$

which is the van't Hoff relationship. (An exothermic reaction has a positive slope on the log(K) vs 1/T plot because $\Delta H_{rxn} < 0$.)

When this is applied to the N ↔ U protein unfolding process:

$$\left[\frac{\partial \frac{\Delta G_{(unf)}}{T}}{\partial \frac{1}{T}}\right]_P = \Delta H_{(unf)} \quad (3)$$

or equivalently

$$\left[\frac{\partial \frac{\Delta G_{(unf)}}{T}}{\partial T}\right]_P = -\frac{\Delta H_{(unf)}}{T^2} \quad (4)$$

Integrating this expression from T^* to T and assuming that the temperature dependence of $\Delta H_{(unf)}$ is equal to $\Delta H^*_{(unf)} + \Delta C_p(T - T^*)$ and $\Delta H^*_{(unf)}$, where the ΔC_p values are all constants over this temperature range

Table 1: Second-Order Oxidation Rate Constants (M^{-1} h^{-1}) of Methionine Residues in Three Short Peptides and rhG-CSF at Different Temperatures at pH 4.0 in 10 mM NaAc Buffer[a]

temp (°C)	free Met[c]	pep1	pep2	pep3	M1	M138	M127	M122
4		9.62 ± 0.70	8.15 ± 0.51	10.10 ± 0.69	7.88 ± 0.69	0.85 ± 0.03	0.78 ± 0.02	0.02 ± 0.00
15		17.98 ± 0.34	16.81 ± 0.19	17.26 ± 0.33	10.80 ± 0.80	2.33 ± 0.06	1.75 ± 0.08	0.06 ± 0.03
20	18.83				14.96 ± 0.71	3.16 ± 0.02	2.40 ± 0.10	0.10 ± 0.01
25[b]	28.19				16.50	6.47	2.73	0.63
30	39.33							
35	57.01							
37		67.59 ± 1.53	63.01 ± 2.48	65.19 ± 1.48	40.61 ± 1.22	6.50 ± 0.23	5.07 ± 0.20	0.38 ± 0.03
45					60.38 ± 4.75	21.61 ± 1.23	19.19 ± 2.75	1.83 ± 0.09
50		123.28 ± 5.79	114.25 ± 3.91	122.19 ± 4.42				
60		344.05 ± 72.65	317.52 ± 58.97	303.77 ± 32.28				

[a] Corresponding methionines in peptides and in rhG-CSF: pep1 with met 122, pep2 with met 127, and pep3 with met 138. [b] Results from Chu et al. (*13*). [c] Results from Yin (*33*).

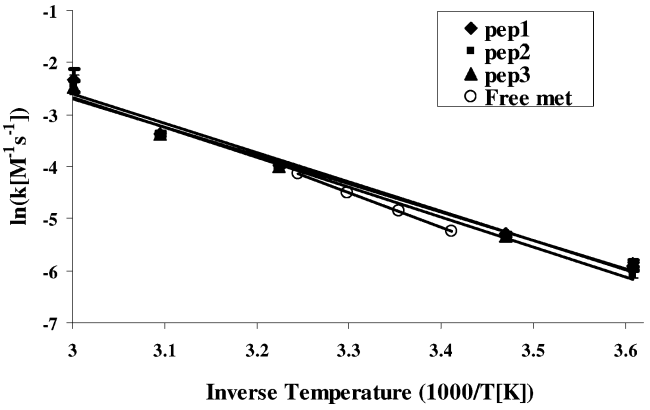

FIGURE 4: Arrhenius plots of the oxidation rate constants of methionine in short peptides as a function of temperature. A good linear relationship was obtained, and the apparent activation energies were obtained from the regression. Error bars are added from Table 1.

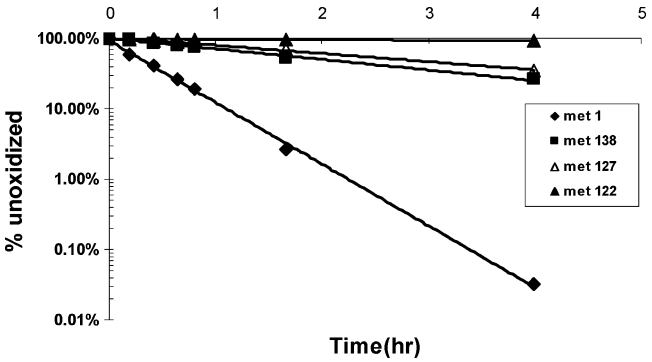

FIGURE 5: Oxidation time-course determined for methionine residues in rhG-CSF. This graph shows the unoxidized percentage of each methionine residue in rhG-CSF, calculated from the peptide map, using the areas of the digested fragment(s). Linear regressions were performed to generate pseudo-first-order rate constants, from which second-order oxidation rate constants were obtained by dividing the former by hydrogen peroxide concentrations.

$$\frac{\Delta G_{(\mathrm{unf})}}{T} - \frac{\Delta G^*_{(\mathrm{unf})}}{T^*} = \frac{\Delta H^*_{(\mathrm{unf})} - \Delta C_p T^*}{T} - \frac{\Delta H^*_{(\mathrm{unf})} - \Delta C_p T^*}{T^*} - \Delta C_p \log\left(\frac{T}{T^*}\right) \quad (5)$$

If we take T^* to be T_m, the melting temperature, then $\Delta G^*_{(\mathrm{unf})} = 0$, so

$$\Delta G_{(\mathrm{unf})} = \Delta H^\circ_{(\mathrm{unf})} - T\frac{\Delta H^\circ_{(\mathrm{unf})}}{T_m} + \Delta C_p\left[T - T_m - T\log\left(\frac{T}{T_m}\right)\right] \quad (6)$$

or for the U ↔ N folding process

$$\Delta G_{(\mathrm{folding})} = \Delta H^\circ_{(\mathrm{folding})} - T\frac{\Delta H^\circ_{(\mathrm{folding})}}{T_m} + \Delta C_p\left[T - T_m - T\log\left(\frac{T}{T_m}\right)\right] \quad (7)$$

The individual Gibbs free energy changes of folding at each temperature are plotted versus temperature according to the Gibbs−Helmholtz equation, as shown in Figure 8. In Table 4, the parameters obtained from the fitting to both CD and fluorescence data are listed. The difference is the manifestation that the two techniques track different events during the protein folding−unfolding process.

DISCUSSION

Comparative Kinetic Analysis of the Oxidation of Methionine Residues. Short peptides each containing one methionine residue were designed to have the same amino acid sequences corresponding to the sequences around each methionine residue in rhG-CSF. Comparison between the oxidation kinetics of corresponding methionine residues in peptides and in the protein can provide information about how protein tertiary structure influences oxidation reactions. Figure 9 shows Arrhenius plots of the oxidation rates of specific methionine residues within the intact protein versus the corresponding peptide. The oxidation rates within the intact protein were generally slower than within the corresponding peptides, presumably due to steric interference, reduced flexibility, and limited diffusion of reactive oxidation species to the methionine site. In addition, the extent of structural influence depends on the specific location of such a residue, possibly determined by the microenvironment around it. Observing these differences, we address the following questions.

(1) How can we understand the structural effects on oxidation kinetics?

(2) Why does the additional complexity of structural effects that supposedly would result in non-Arrhneius oxidation kinetics still yield Arrhenius temperature dependence in the temperature ranged that is examined?

Table 2: Activation Energies and Prefactors of Methionine Oxidation in Three Short Peptides and rhG-CSF at pH 4.0 in 10 mM NaAc Buffer

	free Met	pep1	pep2	pep3	M1	M138	M127	M122
ΔE (kcal/mol)	13.1 ± 0.0	11.1 ± 0.9	11.3 ± 0.8	10.8 ± 0.8	9.1 ± 0.9	12.5 ± 1.7	12.3 ± 1.7	18.8 ± 3.4
$\log_{10}(A)$ (M^{-1} s^{-1})	7.5 ± 0.2	6.2 ± 0.6	6.3 ± 0.6	5.9 ± 0.6	4.4 ± 0.7	6.3 ± 1.2	6.0 ± 1.2	9.6 ± 2.5

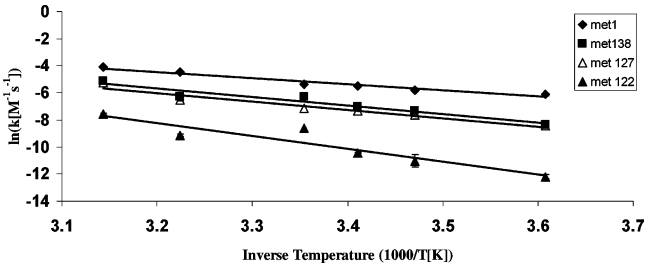

FIGURE 6: Arrhenius plots of oxidation rate constants of methionine in rhG-CSF as a function of temperature. A good linear relationship was obtained, and the activation energies were obtained from the regression. Error bars are added as in Table 1.

(3) Can a simple phenomenological model(s) be developed to account for the structural effects on oxidation rate constants, including its temperature dependence? The model needs to agree with the experimental kinetic data for both peptides and protein. Moreover, a reasonable model needs to have the ability to be reduced back to the case of peptides when the protein loses its structure.

Relationship between Structure and Oxidation Kinetics at Different Temperatures. Unlike reactions involving only small molecules, reactions of macromolecules such as proteins are complicated by their tertiary structure. A reaction involving a buried residue in the hydrophobic core is obviously much slower than one exposed freely in solvent, where another reactant can access it to form a reaction complex. The effect of temperature on the reaction kinetics is also different for reactions involving small molecules versus those involving macromolecules. Specifically, reactions involving macromolecules could involve significant changes in their conformation that in turn could influence the reactivity of a specific reaction group. The structural effect on macromolecular reactions has not been fully elucidated, in part because the structural changes in macromolecules such as proteins are difficult to characterize. The structural changes can be classified into categories according to their relative magnitude.

(1) Thermal motion is the energy change on the order of *kT* that results from finite temperature fluctuations due to the fact that protein molecules can assume a large number of nearly isoenergetic conformations, so-called "conformational substate" (*24*).

(2) Loss of partial/local structure manifests as the energy changes greater than *kT* in which local structure undergoes a significant change, such as loss of helical structure or local denaturation.

(3) Denaturation is a global structure change with a much larger energy change where many interactions contribute to the energy difference.

All these changes will have different effects on reaction kinetics depending on where the specific reaction group is located.

Figure 10 is a hypothetical schematic showing the free energy versus some reaction coordinate in the course of methionine oxidation. Depending on whether a stable intermediate can form after the oxidant molecule accesses the reaction site, two situations are described. The origin of structural effects observed in experiments is explained by a reaction barrier, the height of which depends on the location and microenvironment within the protein structure. In the "oxidant-bound intermediate" model depicted in Figure 10a, a stable intermediate, [P−S···O], is formed between protein P with its thioether sulfur S in a methionine residue and oxidant molecule O. The protein structure poses a free energy barrier to the formation of the [P−S···O] intermediate. There might be multiple such barriers (not drawn in the figure) between the initial state, where oxidant molecules are free in solution and the final state, and where the stable intermediate is formed and ready for the reaction to take place. Blue curves describe cases for a methionine residue in short peptides, while black and red describe the case in which the methionine residue is more and less buried, respectively. Alternatively, in the "non-oxidant-bound intermediate" model shown in Figure 10b, no stable intermediate is required for the intrinsic reaction to occur for oxidation of methionine residues under the influence of protein structure. Situations represented by (a) the oxidant-bound intermediate model and (b) the non-oxidant-bound intermediate model in Figure 10 correspond to the phenomenological models a and b, respectively, in Figure 11.

Phenomenological Models for the Relationship between Protein Structure and Oxidation Kinetics. As mentioned previously, the presence of conformational features for different methionine residues results in disparate oxidation rates, which are also quite different from those in short peptides at a given temperature. Such phenomenological models can account for the conformational influence on oxidation kinetics and therefore result in a mechanistic description of the process. Three models are shown in Figure 11. In the oxidant-bound intermediate model shown in Figure 11a, the oxidation proceeds through an intermediate state which is a complex formed by the binding of oxidant O and protein after the oxidant molecule becomes close to the sulfur site. Alternatively, the non-oxidant-bound intermediate model in panel b depicts the oxidation of sequestered methionine residues in a protein with a complex structure requiring the local structural changes. In the "effective oxidant concentration" model shown in panel c, the oxidant concentration near the methionine site is not equal to its bulk concentration but rather an effective concentration $[O]_{eff}$. Here, the equilibrium distribution of oxidant inside and outside the local region of the protein is described by a Gibbs free energy, ΔG, much like the preferential binding/exclusion Gibbs free energy (*25*).

For the models described above, one can obtain the apparent second-order rate constants (see the Appendix for the detailed derivations).

For the oxidant-bound intermediate model in panel a

Table 3: Data from CD and Tryptophan Fluorescence following Equilibrium Denaturation of rhG-CSF at Different Temperatures at pH 4.0 in 10 mM NaAc Buffer

	tryptophan fluorescence[a]			CD results[b]		
temp (°C)	$\Delta G_{unfolding}$ (kcal/mol)	*m* value[c] (kcal M^{-1} mol^{-1})	c_m value[c] (M)	$\Delta G_{unfolding}$ (kcal/mol)	*m* value[c] (kcal M^{-1} mol^{-1})	c_m value[c] (M)
2	9.74	3.21	3.02	7.86	2.84	2.75
4	11.58	3.79	3.06			
4.5				8.47	2.95	2.86
7	11.16	3.61	3.10	9.38	3.15	2.75
10	11.18	3.57	3.15	9.71	3.08	3.16
15	11.08	3.50	3.18	10.01	3.23	3.12
20[d]	9.00	2.85	3.15	9.27	3.08	3.02
25	9.06	2.94	3.09	8.19	2.72	3.23
30	9.25	3.05	3.05	7.48	2.65	3.04
34	7.42	2.55	2.92			
37	5.84	2.25	2.61	6.75	2.65	2.83

[a] Fluorescence data were recorded for a sample containing 0.5 mg/mL rhG-CSF in 10 mM NaAc at pH 4.0. [b] CD data were reorded for a sample containing 0.02 mg/mL rhG-CSF in 10 mM NaAc at pH 4.0. [c] Values follow from ref *22*. [d] Compare with result from Brems (*21*) with a $\Delta G_{unfolding}$ of 9.0 ± 0.3 kcal/mol under similar conditions.

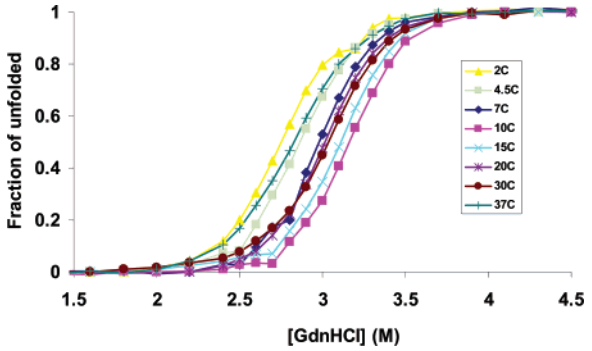

FIGURE 7: Fraction unfolded vs denaturant GdnHCl concentration at different temperatures as indicated, converted and fitted from the CD signal at 222 nm.

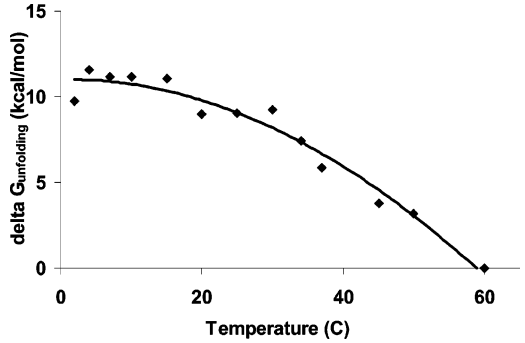

FIGURE 8: Fit of the Gibbs free energy change vs temperature according to the Gibbs−Helmholtz equation. Results were obtained from fluorescence equilibrium denaturation experiments and also from CD experiments. All equilibrium denaturation experiments were conducted in 10 mM sodium acetate buffer at pH 4.0.

$$r_{overall} = \frac{k_{int}}{[O]_0} \frac{1}{1 + \frac{c^{\varnothing}}{[O]_0} e^{(\Delta G)/(RT)}} [O]_0([I] + [N]) \quad (8)$$

For the non-oxidant-bound intermediate model in panel b

$$r_{overall} = \frac{1}{1 + e \frac{\Delta G^{(l)}_{(unf)}}{RT}} k_{int}[O]_0([A] + [N]) \quad (9)$$

For the effective oxidant concentration model in panel c

Table 4: Parameters Fitted from CD and Tryptophan Fluorescence Data According to the Gibbs−Helmholtz Equation

	$\Delta H°_{folding}$ (kcal/mol)	T_m (°C)	ΔC_p (kcal mol^{-1} K^{-1})
fluorescence	−123.1	58.9	−1.95
CD	−131.4	59.6	−2.68

$$r_{overall} = [k_{int} e^{-(\Delta G_{exclusion})/(RT)}][O]_0[N] \quad (10)$$

where [X] denotes the concentration of species X with the subscript meaning initial concentration ($t = 0$), where X can be O (oxidant), I (bound intermediate), N (native protein), or A (unbound intermediate), k_{int} is the intrinsic oxidation rate constant of methionine when there is no structural effect or, more specifically, the oxidation rate constant of the methionine residue in the short peptide, $c^{\varnothing}$ is the concentration of the reference solution, taken to be 1 M, and ΔG is the standard state Gibbs free energy change, with subscripts or superscripts indicating different conditions, defined in the Appendix.

Therefore, under the condition in which the oxidant is in large excess, the reaction can be considered to be pseudo-first-order. Including structural effects decreases the apparent rate constant, consistent with the experimental observation described above (Table 1). In addition to these observations, nonlinear least-squares fitting to three phenomenological models was performed. The objective function is defined as

$$\min_{\Delta H, \Delta C_p} \left(\sum_{T_i} \{\ln[k_j(T_i)] - \ln(k_{j,T_i})\}^2\right) \quad (11)$$

where k_{j,T_i} is the experimental rate constant for methionine residue j at temperature T_i and $k_j(T_i)$ is the rate constant calculated from any model by substituting the Gibbs−Helmholtz equation for the Gibbs energy of structure effect

$$\Delta G = \Delta H - \frac{T}{T_m} \Delta H + \Delta C_p \left[T - T_m - T \log\left(\frac{T}{T_m}\right)\right] \quad (12)$$

In the fitting, T_m is fixed at the melting temperature, 60 °C, for rhG-CSF under the buffer condition under which the oxidation experiments were performed. The results of the least-square nonlinear fit are shown in Figure 12 for each

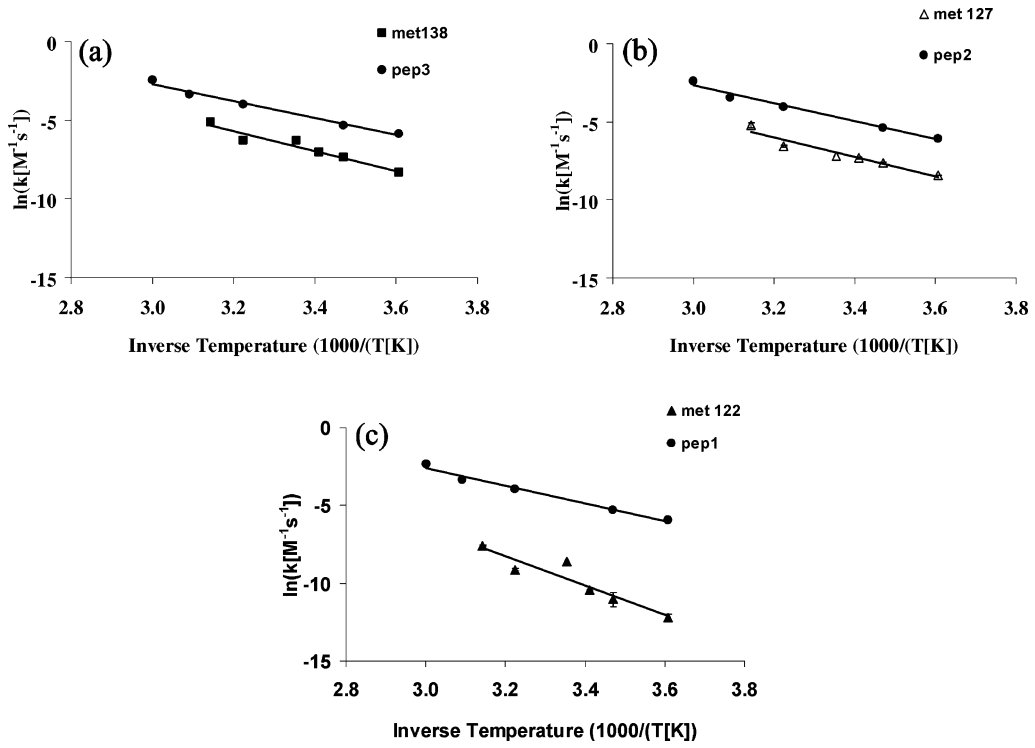

FIGURE 9: Comparisons of the oxidation of methionine residues in rhG-CSF and those in corresponding peptides on the Arrehnius plot: (a) Met 138 and pep3, (b) Met 127 and pep2, and (c) Met 122 and pep1. Lines across each set of data points represent the fit to the Arrhenius equation.

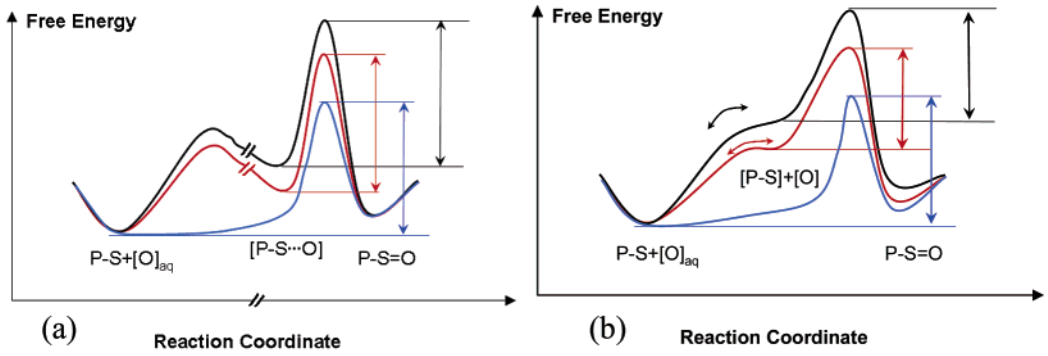

FIGURE 10: Free energy diagram of oxidation of methionine residues: (a) oxidant-bound intermediate model and (b) non-oxidant-bound intermediate model.

methionine residue. All three models fit the rate constants measured reasonably well.

To distinguish the models on the basis of experimental kinetics data, the rate-controlling process governing methionine oxidation needs to be identified. One difficulty in doing so is the lack of a known functional form for the changes in Gibbs free energy associated with the structural effects. By fitting the experimental data, one can choose ΔC_p as any order of polynomial function of temperature to obtain an optimal degree of agreement (in Table 5 and Figure 12, ΔC_p was chosen as a linear function of temperature). However, this approach does not provide mechanistic insight. Such insight could be obtained from molecular simulation, as in previous work (*13*, *17*).

As shown in Figure 13, two different ways of plotting the data are used to reveal the structural effect on the oxidation of methionine residues in rhG-CSF, based on, for example, the non-oxidant-bound intermediate model in Figure 11. We assume the intrinsic oxidation rate constant k_{int} in eq 9 to be that obtained from peptide oxidation

$$k_{int} = k_{peptides} \tag{13}$$

The following expression can be easily derived

$$\ln\left(\frac{k_{peptide}}{k_{apparent}} - 1\right) = \frac{\Delta G^{(l)}_{unf}}{RT} \tag{14}$$

Therefore, by plotting $\ln(k_{peptide}/k_{apparent} - 1)$ versus $1/T$, we can obtain the temperature dependence of $\Delta G^{(l)}_{unf}$, i.e., $\Delta G^{(l)}_{unf}$ as a function of T, shown in the left panel of Figure 13. In Figure 13b, the oxidation rate constant ratios of methionine residue in rhG-CSF with its corresponding peptide are plotted with a scaled Gibbs free energy of denaturation. As the temperature increases, the oxidation rate ratios of the intact protein and the corresponding peptides

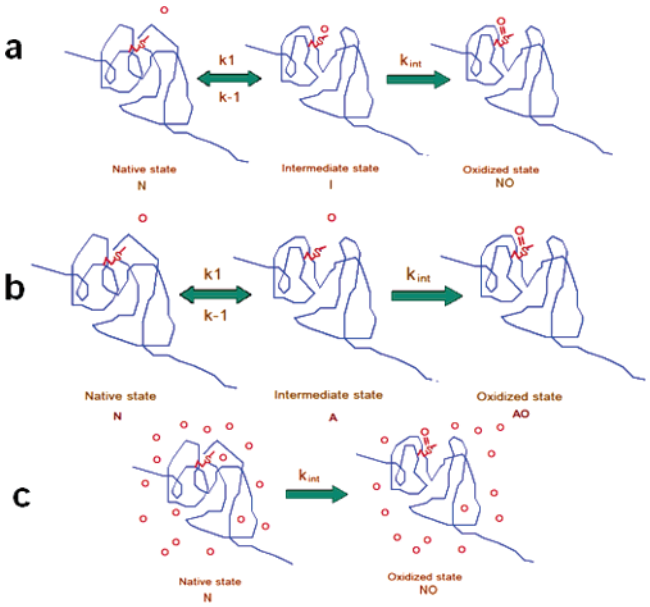

FIGURE 11: Phenomenological models that account for the influence of protein structure on oxidation kinetics. S represents the sulfur site in methionine residues, O a small molecule-oxidizing reagent such as hydrogen peroxide, and S═O the methionine sulfoxide bond formed in the oxidation process: (a) oxidant-bound intermediate model, (b) non-oxidant-bound intermediate model, and (c) effective oxidant concentration model.

also increase and approach the ideal value of 1 (although still much less than 1). Concomitantly, as the Gibbs free energy drops, the oxidation rate ratio approaches zero, which is its value at the melting temperature.

As the temperature increases, the difference in the rate constants for oxidation of corresponding methionine residues in peptides and in protein becomes smaller, since the protein gradually loses its compact structure. At the point of thermal unfolding, the methionine residue has essentially the same microenvironment as the peptide, and the oxidation rate constants should become similar. Thus, we may consider the convergence of the lines in Figure 9 at some higher temperature. However, clearly the Arrhenius lines of Met 138 and Met 127 are almost parallel to the lines of their corresponding peptides, and the line of Met 122 will intersect with that of pep1 at a temperature (~220 °C) much higher than the melting temperature of rhG-CSF (~60 °C). Therefore, we hypothesize that near the melting temperature of rhG-CSF, the structural effects are eliminated or at least minimized, and methionine oxidation kinetics will exhibit non-Arrhenius behavior, deviating from these Arrhenius lines significantly. Unfortunately, this is difficult to test experimentally for rhG-CSF due to the fact that rhG-CSF has a great propensity to aggregate at temperatures approaching the thermal melting temperature of 60 °C.

The non-oxidant-bound intermediate phenomenological model b can illustrate the expectations described above. Parameters fitted from oxidation rate constants in the experimental temperature range were used to extrapolate the Arrhenius lines to a temperature range near T_m and even beyond, as shown in Figure 14. Even though the non-oxidant-bound intermediate model can produce the expected behavior near T_m and beyond, there is some sacrifice in the fitting of experimental data, as quantified in Table 6.

Analysis Based on Activation Energy Differences. As shown in Table 2, there are statistically significant differences among the activation energies. We suggest these differences are the manifestation of structural effects on the basis of previous studies (*13*) in which it was concluded that without structural hindrance on the accessibility of water molecules, there would be equal activation barrier energies for all four methionines in rhG-CSF when oxidized by hydrogen peroxide. The non-oxidant-bound intermediate model in Figure 11 is now taken, as an example, to account for the differences in activation energies among methionine residues in rhG-CSF. Similar analyses can be done for the other models.

If one assumes that k_{int} follows the Arrhenius equation $k_{int} = Ae^{-(\Delta E^{\dagger})/(RT)}$, where the constant A has units of inverse seconds, then

$$k_{apparent} = \frac{Ae^{-(\Delta E^{\dagger})/(RT)}}{1 + e^{(\Delta^{G_{unf}(l)})/(RT)}} \tag{15}$$

Notice that there are two limits for this apparent rate constant expression.

(1) When $-\Delta G_{unf}^{(l)} \ll RT$, then

$$k_{apparent} = Ae^{-(\Delta E^{\dagger})/(RT)} \tag{16}$$

(2) When $-\Delta G_{unf}^{(l)} \gg RT$

$$k_{apparent} = Ae^{-[\Delta E^{\dagger} + \Delta^{G_{unf}(l)}]/(RT)} = Ae^{-(\Delta E_{apparent})/(RT)} \tag{17}$$

In both cases, the apparent reaction rate can be simplified to an Arrhenius equation. In case 2, the apparent activation energy contains the contribution from the local structural change. The activation energy difference between each methionine in rhG-CSF and that in the corresponding peptide can be treated as the local folding free energy. Actually, this activation energy difference can be used to ascertain whether the methionine oxidation is locally or globally dependent on structure with respect to temperature, as follows:

$$\begin{cases} \text{no structural dependence, when } -\Delta G_{unf}^{(l)} \ll RT \\ \text{local structural dependence, when } -\Delta G_{unf}^{(l)} \sim RT \\ \text{global structural dependence, when } -\Delta G_{unf}^{(l)} \gg RT \end{cases}$$

As for methionine oxidation in rhG-CSF, it can be seen (in Table 2) that the activation energy difference in Met 122 and Met 1 in rhG-CSF is at least 3 kcal/mol, which is much larger than RT (0.549−0.659 kcal/mol) over the temperature range that was tested (4−60 °C). Therefore, the latter extreme scenario is applicable in that the oxidation of Met 122 in rhG-CSF has global structural dependence. However, Met 127 and Met 138 display intermediate values of activation energy difference, which may imply that they have a local structural dependence on the oxidation reaction.

The analysis given above cannot account for the unexpected smaller activation energy of Met 1 in rhG-CSF. Perhaps the negative charge on the C-terminus impacts methionine oxidation, based on the difference between Met 1 and free methionine and the other methionine residues in rhG-CSF or peptides, where methionine residues are either negatively charged or bonded to neighboring residues. The protonation states of both the N-terminus and the C-terminus of the methionine residue could affect the organization of

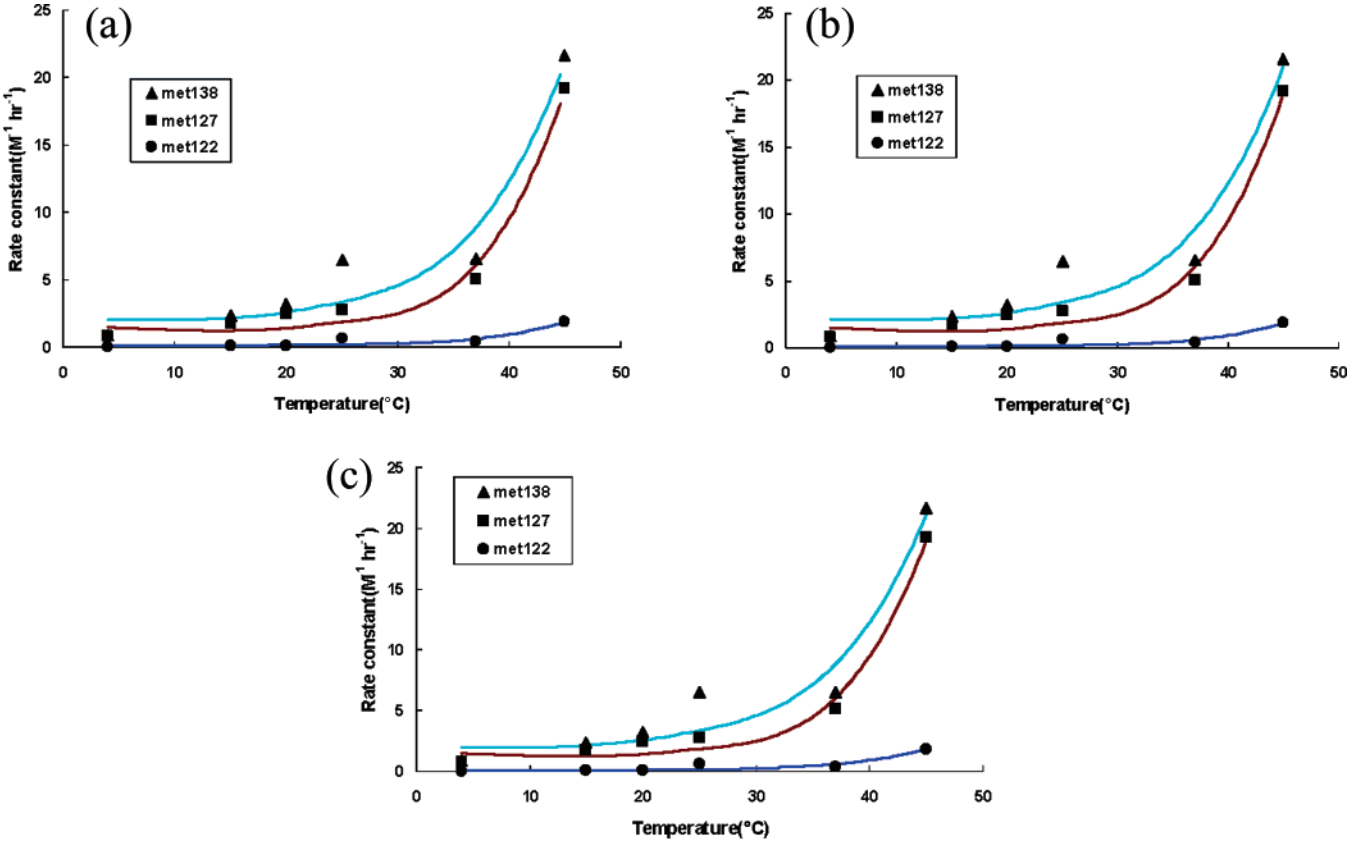

FIGURE 12: Results of least-square fits to (a) the oxidant-bound intermediate model, (b) the non-oxidant-bound intermediate model, and (c) the effective oxidant concentration model correspond to those presented in Figure 11. Lines across each set of data points represent the fit to the three models.

Table 5: Least-Squares Nonlinear Fits of Model Parameters

		$\Delta H^{local}_{folding}$ (kcal/mol)	$\Delta C^{local}_{pfolding}$ (kcal °C^{-1} mol^{-1})
model a	met138	−22.7	−0.5
	met127	−28.1	−0.7
	met122	−52.7	−1.2
model b	met138	−20.3	−0.5
	met127	−26.7	−0.7
	met122	−52.3	−1.1
model c	met138	−22.7	−0.5
	met127	−28.1	−0.7
	met122	−52.7	−1.2

the water network, which plays an essential role in oxidation kinetics (*15*, *25*), and give rise to differences in apparent Arrhenius parameters.

Implications for Biochemistry. To our knowledge, the dependence of chemical kinetics on temperature of the general type of reaction studied in this work has not been previously published. There is similar methionine oxidation work on the protein IL-1RA (*26*). Others studied the accessibility of cysteine residues in IL-1RA (*27*) and G-CSF and other proteins (*28*, *29*). Still, in general, there has been difficulty in the characterization of the complex structure of the protein molecule and the structural effects on the reaction rate. However, there are many examples where the complex structure of protein molecules plays a similar and essential role in chemical reactivity. Start and Stein (*30*) studied the alkylation of methionine residues in ribonuclease A by iodoacetate or iodoacetamide and found that only at low pH or in the presence of denaturant could rapid alkylation occur. They also found that under the condition when the protein is unfolded, the alkylation rates for different methionine residues are nearly the same. This can be explained by the free energy barrier posed by protein structure being too large to overcome unless the structure of protein molecules is perturbed. An equivalent rate of reactivity at various sites within the unfolded protein indicates that the intrinsic reaction barrier is similar for different methionines. As another example, *tert*-butyl hydrogen peroxide oxidizes methionine residues much slower than hydrogen peroxide (*31*). Despite possible differences in oxidizing capability, *tert*-butyl hydrogen peroxide is larger in terms of molecular volume. This effectively increases the energy barrier posed by protein structure and also destabilizes the intermediate state. Liu et al. (*32*) found that testicular cytochrome *c* in the ferrous state has a slower rate of oxidation by hydrogen peroxide than its counterpart in somatic cells due to changes in protein structure, as indicated by differing water patterns inside the protein structure and the interactions between the heme group and its surrounding residues. The origin of this difference is also expected to be explained in the framework of this study. In addition, the model and theory developed here were also tested on another protein IL-1RA (*26*), with which the only data of methionine oxidation rate constants as a function of temperature could be found, and were confirmed for their applicability (data not shown).

Experimentally measured rate constants can be fit with several plausible phenomenological models, such as those presented in this paper. However, it is difficult to ascertain which model is correct due to the lack of knowledge about the structure dynamic or equilibrium properties of a local region around methionine residues in the complex structure

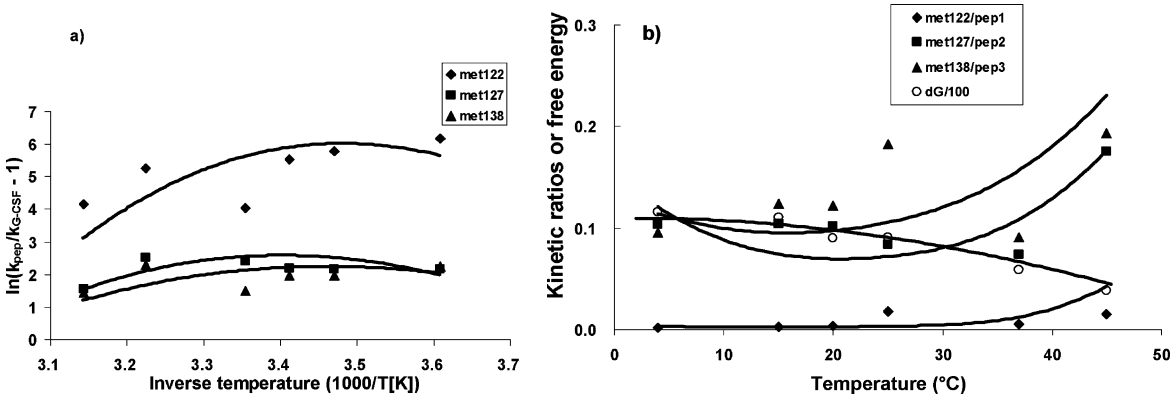

FIGURE 13: Comparative kinetic data of three short peptides and methionine residues in rhG-CSF. (a) Ln($k_{peptide}/k_{apparent} - 1$) vs $1/T$ for three methionine residues in rhG-CSF. Solid lines represent fittings by eq 9 using parameters from Table 5. (b) Ratios of oxidation rate constants of methionine residues in rhG-CSF with its corresponding peptide are plotted with a scaled Gibbs free energy of denaturation. Solid lines represent fittings by eq 9 using parameters from Table 5 and fitting by eq 7.

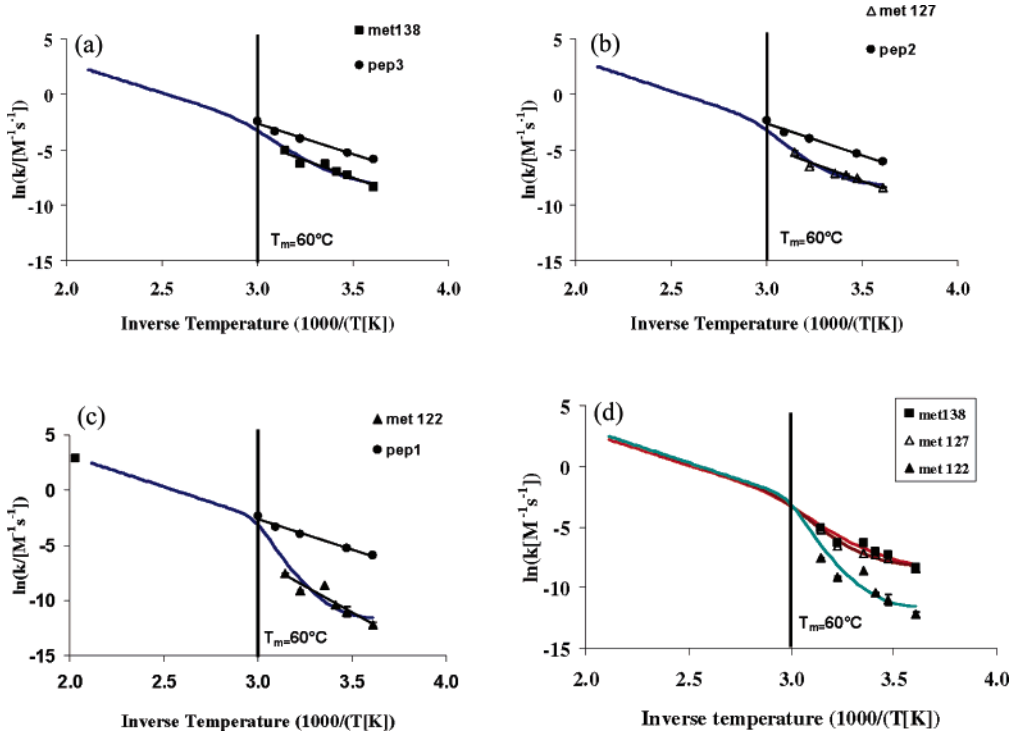

FIGURE 14: Comparison of the Arrhenius fit and the non-oxidant-bound intermediate model fit: (a) Met 138 and pep3, (b) Met 127 and pep2, (c) Met 122 and pep1, and (d) all together. Dashed lines in panels a−c represent the direct extrapolations of Arrhenius lines for methionine residues in rhG-CSF. Curved lines represent the predicted behavior of the non-oxidant-bound intermediate model.

Table 6: Comparisons of Standard Deviations (SD) Calculated from the Arrhenius Equation versus Experimental Rate Constants and Those Calculated from Model b versus Those from Experiment

	Met 138	Met 127	Met 122
SD for ln(k) − ln(k_Arrhenius)	0.28	0.28	0.58
SD for ln(k) − ln(k_model b)	0.41	0.30	0.96

of a protein molecule. A possible direction for obtaining such information can be intrinsic fluorescence via substitution of a tryptophan residue at the methionine site. The dynamics of local structure likely has a strong influence on the reactivity and reaction rate. The understanding of local structural motions not only will be crucial to studies like methionine oxidation but also can be applied to protein aggregation, ligand transport and binding, and enzymatic catalysis.

The models developed here were aimed at the understanding the "dual" role that temperature plays in methionine oxidation in protein molecules, that is, how temperature affects chemical kinetics intrinsically and affects protein conformation secondarily. These models have some minimal requirements, such as a reasonable explanation of the apparent Arrhenius behavior of oxidation of methionine residues in rhG-CSF over the temperature range that was examined and restoration of the simple Arrhenius behavior when protein structural effects become minimal at temperatures much higher than the melting temperature. When all of these requirements are taken into account, the models are expected to cover a wider range of temperature. In essence, the modeling presented in the paper puts into proper context both the kinetics of oxidation and our understanding of protein conformational changes by presenting mathematically

Table 7: Degradation of rhG-CSF (in percentage) Estimated from Kinetic Data at 29 °C in 10 mM Acetate Buffer at pH 4.0

	[hydrogen peroxide]	6 months				12 months				24 months			
		M1	M138	M127	M122	M1	M138	M127	M122	M1	M138	M127	M122
prediction from measured rate constant	0.4 μM	4%	1%	1%	0%	8%	2%	2%	0%	16%	4%	3%	0%
	1 μM	10%	3%	2%	0%	20%	5%	4%	0%	35%	10%	7%	1%
	10 μM	66%	23%	18%	1%	89%	41%	32%	3%	99%	65%	54%	6%
	0.1 mM	100%	93%	85%	13%	100%	99%	98%	25%	100%	100%	100%	44%
	1 mM	100%	100%	100%	76%	100%	100%	100%	94%	100%	100%	100%	100%
measured[a]	0.19 μM active oxygen with 0.38 μM H_2O_2		$2.5 \pm 1.0\%$[b]		$2.6 \pm 1.4\%$		$2.9 \pm 0.8\%$[b]		$2.8 \pm 1.0\%$				

[a] Long-term experimental data provided by Amgen Inc., performed using a commercial formulation buffer. [b] Sum of the percentage of oxidation of both Met 127 and Met 138.

the physical basis of the oxidation of methionine residues in proteins. Because our models have a physical basis, we expect them to be generally applicable.

Implications for Pharmaceutical Shelf Life Prediction. An important criterion for protein pharmaceutical formulations is stabilization using an appropriate buffer, isoosmotic additives, and other excipients under optimal temperature and pH conditions. Since the desired shelf life is typically 18−24 months and degradation pathways such as oxidation usually occur very slowly over the course of that time frame, it is highly desirable to have a rapid shelf life prediction method for screening formulations. One way of accelerating oxidation is to elevate the temperature. Therefore, development of a model for predicting oxidation at low temperatures using data at high temperatures will facilitate predicting protein shelf life. Quantifying the effect of protein structure on chemical kinetics is a prerequisite for such prediction. One major assumption with the model developed here is that the oxidation pathway using the oxidizing chemical species (H_2O_2) among reactive oxygen species is similar to oxidation in the absence of H_2O_2. Likewise, accelerated oxidation at higher temperatures should be predictive of oxidation at lower temperatures. In addition, the model does not capture any other significant competing degradation pathways, such as aggregation, which is inevitably problematic in the shelf life studies at temperatures elevated above the storage temperature.

A critical unknown parameter in oxidation studies is the level of peroxides in the formulation buffer. In Table 7, the amount of rhG-CSF degradation is shown at various hydrogen peroxide levels (from micromolar to millimolar) and at different time lengths (from 6 to 24 months) in storage buffer. The estimation is based on the experimental rate constants at 29 °C from forced oxidation at which some long-term experimental data are available. Peroxide levels of several micromolar match experimental data reasonably well. This suggests that an accurate estimate of shelf life can be made using appropriate concentrations of hydrogen peroxide and active oxygen species experimentally measured as inputs in addition to the kinetic data of accelerated oxidation at high temperatures. Thus, forced oxidation studies at elevated storage temperatures can guide rational formulation of protein pharmaceuticals against oxidative degradation.

CONCLUSIONS

In this work, we studied the temperature dependence of oxidation rate constants of methionine residues in several chemically synthesized peptides and in recombinant human granulocyte colony-stimulating factor (rhG-CSF) by hydrogen peroxide (H_2O_2). Experiments aimed at exploring the equilibrium denaturation of rhG-CSF also were conducted, and Gibbs free energies of unfolding as a function of temperature were calculated on the basis of experimental data. We found significant variation among the oxidation rate constants for different methionine residues in rhG-CSF and as a function of temperature. The rate constants for each methionine residue can be fit reasonably well according to the Arrhenius equation. This suggests that degradation is governed by the intrinsic oxidation reaction rather than a local conformational event having a complex temperature dependence. We also found that if we assume the existence of an additional activation free energy barrier due to the transport of oxidant molecule H_2O_2, a more complicated, non-Arrhenius equation ensues. However, this equation simplifies to the Arrhenius equation under certain circumstances. We classified the methionine residues in rhG-CSF according to the degree to which the protein structure affects oxidation kinetics, i.e., no structural dependence, local structural dependence, and global structural dependence. Additionally, three models for considering the structural effect of protein molecules on the oxidation of methionine residues were developed. We found these models can fit the experimental data equally well. The non-oxidant-bound intermediate model, in particular, can produce the anticipated temperature dependence of rate constants near the melting temperature and even beyond, when the influence of protein structure becomes diminishingly small. However, the phenomenological models we considered cannot be distinguished purely on the basis of phenomenological rate constant data. Trusted local dynamical information such as that which could be determined from molecular simulations would be needed. An example in which shelf life prediction of protein pharmaceuticals using the temperature dependence of oxidation rate and model prediction yielded stabilities that matched well was shown.

APPENDIX

For the three phenomenological models shown in Figure 11, the overall rate expressions can be obtained as follows.

In oxidant-bound intermediate model a, the elementary steps hypothesized in the model are as follows:

$$O + N \underset{k_{-1}}{\overset{k_1}{\rightleftharpoons}} I$$

$$I \xrightarrow{k_{int}} NO$$

in which the formation of the intermediate complex of the protein and oxidant is assumed to be reversible. Furthermore, the equilibrium of the first step can be expressed as

$$\frac{[I]}{[N][O]} = \frac{k_1}{k_{-1}} = \frac{K}{c^{\varnothing}} = \frac{e^{-[(\Delta G)/(RT)]}}{c^{\varnothing}} \quad \text{(A-1)}$$

where $c^{\varnothing}$ is the concentration of the reference solution, taken to be 1 M, and ΔG is the standard state Gibbs free energy change.

$$\text{mass conservation: } [I] + [N] + [NO] = [N]_0 \quad \text{(A-2)}$$

$$\text{rate expression: } r_{overall} = \frac{d[NO]}{dt} = k_{int}[I] \quad \text{(A-3)}$$

So that

$$[I] = \frac{[N]_0 - [NO]}{1 + \frac{c^{\varnothing} e^{(\Delta G)/(RT)}}{[O]}} \quad \text{(A-4)}$$

and

$$r_{overall} = \frac{d[NO]}{dt} = k_{int}[I] = k_{int}\frac{[N]_0 - [NO]}{1 + \frac{c^{\varnothing} e^{(\Delta G)/(RT)}}{[O]}} \quad \text{(A-5)}$$

with the initial condition being $[NO]_0 = 0$, and when the oxidant is in great excess ($[N]_0 \ll [O] \approx [O]_0$). Integration yields

$$[NO] = [N]_0(1 - e^{-((k_{int})/\{1+[c^{\varnothing} e(\Delta G)/(RT)]/([O]_0)\})t}) \quad \text{(A-6)}$$

$$[N] + [I] = [N]_0 e^{-((k_{int})/\{1+[c^{\varnothing} e(\Delta G)/(RT)]/([O]_0)\})t} \quad \text{(A-7)}$$

$$r_{overall} = \frac{d[NO]}{dt} = k_{int}\frac{1}{1 + \frac{c^{\varnothing} e^{(\Delta G)/(RT)}}{[O]_0}}([I] + [N]) = \frac{k_{int}}{[O]_0}\frac{1}{1 + \frac{c^{\varnothing}}{[O]_0} e^{(\Delta G)/(RT)}}[O]_0([I] + [N]) \quad \text{(A-8)}$$

For non-oxidant-bound intermediate model b, the assumed elementary steps hypothesized in the model are as follows:

$$N \underset{k_{-1}}{\overset{k_1}{\rightleftharpoons}} A$$

$$A + O \xrightarrow{k_{int}} AO$$

If the structural change is very fast and in equilibrium, the intrinsic oxidation will be the rate-determining step, leading to

$$\frac{[A]}{[N]} = \frac{k_1}{k_{-1}} = K = e^{-[\Delta^{G_{unf(l)}}]/(RT)} \quad \text{(A-9)}$$

$$[A] + [N] + [AO] = [P]_0 \quad \text{(A-10)}$$

One also has

$$r_{overall} = \frac{d[AO]}{dt} = k_{int}[A][O] \quad \text{(A-11)}$$

$$[A] = \frac{k_1([P]_0 - [AO])}{k_1 + k_{-1}} = \frac{[P]_0 - [AO]}{1 + e^{[\Delta^{G_{unf(l)}}]/(RT)}} \quad \text{(A-12)}$$

Therefore

$$r_{overall} = \frac{d[AO]}{dt} = \frac{k_{int}}{1 + e^{[\Delta^{G_{unf(l)}}]/(RT)}}([P]_0 - [AO])[O] = \frac{k_{int}}{1 + e^{[\Delta^{G_{unf(l)}}]/(RT)}}([A] + [N])[O] \quad \text{(A-13)}$$

It can be seen that the apparent rate constant in this model is

$$k_{apparent} = \frac{k_{int}}{1 + e^{[\Delta^{G_{unf(l)}}]/(RT)}} \quad \text{(A-14)}$$

For effective oxidant concentration model c, the oxidant concentration near the methionine site is not equal to its bulk concentration, but rather an effective concentration $[O]_{eff}$. The equilibrium distributions of oxidant inside and outside the protein are described by a Gibbs free energy ΔG, much like the preferential binding/exclusion Gibbs free energy, but used to describe the different distributions of cosolute near protein surface and in bulk solvent.

Therefore, concentrations of oxidant in bulk solvent, $[O]_0$, and that near the methionine site have the equilibrium relationship

$$\frac{[O]_{eff}}{[O]_0} = e^{-(\Delta G_{exclusion})/(RT)} \quad \text{(A-15)}$$

Thus, the phenomenological oxidation rate becomes

$$r_{overall} = k_{int}[O]_{eff}[N] = k_{int}[O]_0 e^{-(\Delta G_{exclusion})/(RT)}[N] \quad \text{(A-16)}$$

Here ΔG contains the information of protein complex structure. Therefore, it can be a complex function of temperature.

ACKNOWLEDGMENT

We thank many people in the Protein Formulation group within the Pharmaceutics Department at Amgen Inc. for their helpful suggestions and discussion along with this project. In particular, we thank Dr. Sampath Krishnan for helpful advice on how to quench the oxidation reaction, Dr. Songpon

Deechongkit for help with the CD instrumentation, and Dr. Baron G. Peters in Trout Group at MIT for discussion about the models.

REFERENCES

1. Chao, C. C., Ma, Y. S., and Stadtman, E. R. (1997) Modification of protein surface hydrophobicity and methionine oxidation by oxidative systems, *Proc. Natl. Acad. Sci. U.S.A. 94*, 2969−2974.
2. Stadtman, E. R. (2001) Protein oxidation in aging and age-related diseases, *Ann. N.Y. Acad. Sci. 928*, 22−38.
3. Trifunovic, A., Hansson, A., Wredenberg, A., Rovio, A. T., Dufour, E., Khvorostov, I., Spelbrink, J. N., Wibom, R., Jacobs, H. T., and Larsson, N. G. (2005) Somatic mtDNA mutations cause aging phenotypes without affecting reactive oxygen species production, *Proc. Natl. Acad. Sci. U.S.A. 102*, 17993−17998.
4. Hokenson, M. J., Uversky, V. N., Goers, J., Yamin, G., Munishkina, L. A., and Fink, A. L. (2004) Role of individual methionines in the fibrillation of methionine-oxidized α-synuclein, *Biochemistry 43*, 4621−4633.
5. Markesbery, W. R. (1997) Oxidative stress hypothesis in Alzheimer's disease, *Free Radical Biol. Med. 23*, 134−147.
6. Watson, A. A., Fairlie, D. P., and Craik, D. J. (1998) Solution structure of methionine-oxidized amyloid β-peptide(1-40). Does oxidation affect conformational switching? *Biochemistry 37*, 12700−12706.
7. Vogt, W. (1995) Oxidation of Methionyl Residues in Proteins: Tools, Targets, and Reversal, *Free Radical Biol. Med. 18*, 93−105.
8. Ciorba, M. A., Heinemann, S. H., Weissbach, H., Brot, N., and Hoshi, T. (1997) Modulation of potassium channel function by methionine oxidation and reduction, *Proc. Natl. Acad. Sci. U.S.A. 94*, 9932−9937.
9. Wei, W. (1999) Instability, stabilization, and formulation of liquid protein pharmaceuticals, *Int. J. Pharm. 185*, 129−188.
10. Anbanandam, A., Urbauer, R. J. B., Bartlett, R. K., Smallwood, H. S., Squier, T. C., and Urbauer, J. L. (2005) Mediating molecular recognition by methionine oxidation: Conformational switching by oxidation of methionine in the carboxyl-terminal domain of calmodulin, *Biochemistry 44*, 9486−9496.
11. Kim, Y. H., Berry, A. H., Spencer, D. S., and Stites, W. E. (2001) Comparing the effect on protein stability of methionine oxidation versus mutagenesis: Steps toward engineering oxidative resistance in proteins, *Protein Eng. 14*, 343−347.
12. Nguyen, T. H. (1994) Oxidation Degradation of Protein Pharmaceuticals, in *Formulation and Delivery of Proteins and Peptides* (Cleland, J. L., and Langer, R., Eds.) pp 59−71, American Chemical Society, Washington, DC.
13. Chu, J. W., Yin, J., Wang, D. I. C., and Trout, B. L. (2004) Molecular dynamics simulations and oxidation rates of methionine residues of granulocyte colony-stimulating factor at different pH values, *Biochemistry 43*, 1019−1029.
14. Griffiths, S. W., and Cooney, C. L. (2002) Relationship between protein structure and methionine oxidation in recombinant human α1-antitrypsin, *Biochemistry 41*, 6245−6252.
15. Chu, J. W., and Trout, B. L. (2004) On the mechanisms of oxidation of organic sulfides by H_2O_2 in aqueous solutions, *J. Am. Chem. Soc. 126*, 900−908.
16. Chu, J. W., Yin, J., Brooks, B. R., Wang, D. I. C., Ricci, M. S., Brems, D. N., and Trout, B. L. (2004) A comprehensive picture of non-site specific oxidation of methionine residues by peroxides in protein pharmaceuticals, *J. Pharm. Sci. 93*, 3096−3102.
17. Chu, J. W., Yin, J., Wang, D. I. C., and Trout, B. L. (2004) A structural and mechanistic study of the oxidation of methionine residues in hPTH(1-34) via experiments and simulations, *Biochemistry 43*, 14139−14148.
18. Souza, L. M., Boone, T. C., Gabrilove, J., Lai, P. H., Zsebo, K. M., Murdock, D. C., Chazin, V. R., Bruszewski, J., Lu, H., Chen, K. K., Barendt, J., Platzer, E., Moore, M. A. S., Mertelsmann, R., and Welte, K. (1986) Recombinant Human Granulocyte Colony-Stimulating Factor: Effects on Normal and Leukemic Myeloid Cells, *Science 232*, 61−65.
19. Aritomi, M., Kunishima, N., Okamoto, T., Kuroki, R., Ota, Y., and Morikawa, K. (1999) Atomic structure of the GCSF-receptor complex showing a new cytokine-receptor recognition scheme, *Nature 401*, 713−718.
20. Hill, C. P., Osslund, T. D., and Eisenberg, D. (1993) The Structure of Granulocyte-Colony-Stimulating Factor and Its Relationship to Other Growth-Factors, *Proc. Natl. Acad. Sci. U.S.A. 90*, 5167−5171.
21. Brems, D. N. (2002) The kinetics of G-CSF folding, *Protein Sci. 11*, 2504−2511.
22. Tanford, C. (1970) Protein denaturation. C. Theoretical models for the mechanism of denaturation, *Adv. Protein Chem. 24*, 1−95.
23. Lu, H. S., Klein, M. L., and Lai, P. H. (1988) Narrow-Bore High-Performance Liquid-Chromatography of Phenylthiocarbamyl Amino-Acids and Carboxypeptidase-P Digestion for Protein C-Terminal Sequence-Analysis, *J. Chromatogr. 447*, 351−364.
24. Frauenfelder, H., Sligar, S. G., and Wolynes, P. G. (1991) The Energy Landscapes and Motions of Proteins, *Science 254*, 1598−1603.
25. Chu, J. W., Brooks, B. R., and Trout, B. L. (2004) Oxidation of methionine residues in aqueous solutions: Free methionine and methionine in granulocyte colony-stimulating factor, *J. Am. Chem. Soc. 126*, 16601−16607.
26. Thirumangalathu, R., Krishnan, S., Bondarenko, P., Ricci, M. S., Randolph, T. W., Carpenter, J. F., Brems, D. N. (2006) Role of conformational stability in methionine oxidation of recombinant human interleukin-1 receptor antagonist, manuscript in preparation.
27. Roy, S., Katayama, D., Dong, A. C., Kerwin, B. A., Randolph, T. W., and Carpenter, J. F. (2006) Temperature dependence of benzyl alcohol- and 8-anilinonaphthalene-1-sulfonate-induced aggregation of recombinant human interleukin-1 receptor antagonist, *Biochemistry 45*, 3898−3911.
28. Pipes, G. D., Kosky, A. A., Abel, J., Zhang, Y., Treuheit, M. J., and Kleemann, G. R. (2005) Optimization and applications of CDAP labeling for the assignment of cysteines, *Pharm. Res. 22*, 1059−1068.
29. Raso, S. W., Abel, J., Barnes, J. M., Maloney, K. M., Pipes, G., Treuheit, M. J., King, J., and Brems, D. N. (2005) Aggregation of granulocyte-colony stimulating factor in vitro involves a conformationally altered monomeric state, *Protein Sci. 14*, 2246−2257.
30. Stark, G. R., and Stein, W. H. (1964) Alkylation of the Methionine Residues of Ribonuclease in 8 M Urea, *J. Biol. Chem. 239*, 3755−3761.
31. Lu, H. S., Fausset, P. R., Narhi, L. O., Horan, T., Shinagawa, K., Shimamoto, G., and Boone, T. C. (1999) Chemical modification and site-directed mutagenesis of methionine residues in recombinant human granulocyte colony-stimulating factor: Effect on stability and biological activity, *Arch. Biochem. Biophys. 362*, 1−11.
32. Liu, Z., Lin, H., Ye, S., Liu, Q. Y., Meng, Z., Zhang, C. M., Xia, Y., Margoliash, E., Rao, Z., and Liu, X. J. (2006) Remarkably high activities of testicular cytochrome c in destroying reactive oxygen species and in triggering apoptosis, *Proc. Natl. Acad. Sci. U.S.A. 103*, 8965−8970.
33. Yin, J., Chu, J. W., Ricci, M. S., Brems, D. N., Wang, D. I. C., and Trout, B. L. (2004) Effects of antioxidants on the hydrogen peroxide-mediated oxidation of methionine residues in granulocyte colony-stimulating factor and human parathyroid hormone fragment 13−34. *Pharmaceutical Research 21*, 2377−2383.

BI061855C